

High-order maps with acceleration for optimization of electrostatic and radio-frequency ion-optical elements

Andrew A. Geraci

Physics Division, Argonne National Laboratory, Argonne, Illinois 60439 and Department of Physics, Stanford University, Stanford, California 94305

Teresa A. Barlow

Physics Division, Argonne National Laboratory, Argonne, Illinois 60439

Mauricio Portillo

Physics Division, Argonne National Laboratory, Argonne, Illinois 60439 and Department of Physics and Astronomy, Michigan State University, East Lansing, Michigan 48824

Jerry A. Nolen and Kenneth W. Shepard

Physics Division, Argonne National Laboratory, Argonne, Illinois 60439

Kyoko Makino

National Superconducting Cyclotron Laboratory, East Lansing, Michigan 48824 and Department of Physics, University of Illinois at Urbana-Champaign, Urbana, Illinois 61801

Martin Berz

National Superconducting Cyclotron Laboratory, East Lansing, Michigan 48824 and Department of Physics and Astronomy, Michigan State University, East Lansing, Michigan 48824

(Received 7 March 2002; accepted for publication 28 May 2002)

A method has been developed to calculate accurate high-order ion-optical maps for electrostatic and radio-frequency accelerating elements. The method has been incorporated into the arbitrary-order map-based beam optics code COSY Infinity. The treatment is restricted to the case of negligible magnetic fields, as is typical of heavy-ion accelerating cavities, and does not include space charge. For validation purposes, the beam dynamics calculated for these elements is compared against ray tracing for typical beam and cavity parameters. Different from the ray-tracing approach, parameter changes of individual components typically require only recalculation of the maps of the particular components and not the entire system, and thus the method is particularly suitable for optimization. The approach developed for accurate analytical representation of the on- and off-axis electric fields of cylindrically symmetric electrostatic lenses and radio-frequency cavities is described. Some of the many possible applications for using accurate high-order map representations of Einzel lenses, electrostatic accelerating gaps, and radio-frequency accelerating structures are discussed. © 2002 American Institute of Physics. [DOI: 10.1063/1.1497499]

I. INTRODUCTION

A wide variety of sophisticated beam transport systems, ion-optical spectrographs, and linear accelerators based on independently phased superconducting resonators cannot be designed or optimized to high order by the current generation of matrix- or map-based transport codes in high energy and nuclear physics. For many such systems it is typical to start with a first- or second-order simulation to obtain the initial tune or layout, and to follow that by detailed ray-tracing simulations for parameter optimization to higher order. In this work, we extend the formulation of an arbitrary-order beam optics code to include maps for acceleration and focusing with dc and time-varying electric fields. The fields are obtained from a Poisson solver for cylindrically symmetric systems of arbitrary geometry. The new beam-optical components include elements such as Einzel lenses, dc accelerating gaps, and radio-frequency (rf) accelerating structures such as superconducting resonators.

Map-based beam optics provides an approach conducive

to optimization, in that the transfer map explicitly displays and isolates order-by-order dependence on coordinates. Furthermore, most parameter changes occurring in the process of optimization affect only the local transfer map of the affected element and do not necessitate recomputation of the entire system, which increases simulation efficiency. The arbitrary order map-based beam optics code COSY Infinity¹ is equipped with fitting algorithms, and further can readily compute the effects of small changes in system parameters on the dynamics. However, previous versions of the code were not equipped to deal with elements having general field profiles that produce a net change in particle energies. In this article we generalize COSY Infinity to calculate transport maps to arbitrary order including the effects of such elements. The extended map-oriented beam optics code is useful in the design and optimization of a variety of beam transport and acceleration systems including arrays of independently phased superconducting resonators for advanced ion linacs as described below.

We have also developed a method for accurate evalua-

tion of high-order maps of elements consisting of cylindrically symmetric electrodes with realistic geometries. An analytic expression for the on-axis electric potential is generated via a Poisson solver and the off-axis fields are then generated to higher and higher accuracy by an order-by-order fixed point iteration of differential algebraic (DA) vectors. This DA approach for generating off-axis fields is further discussed in the Appendices. The beam dynamics calculated for sample elements is compared against ray tracing to illustrate the accuracy of the map methods at various orders.

Finally, we include a section describing a variety of applications of this work to ion-optical systems that include electrostatic lenses or rf accelerating cavities. Although the examples considered have cylindrical symmetry, the formalism employed for evaluating high-order maps with acceleration can in principle be extended to more general three-dimensional (3D) field configurations, provided the reference trajectory is straight or planar. Extension to nonplanar curvilinear coordinates such as those described in Ref. 2 is also possible after suitable modifications.

II. IMPLEMENTATION OF ACCELERATION AND TIME-VARYING FIELDS

In matrix-oriented beam optics, the beam is regarded as an ensemble of particles with similar classical phase space coordinates.³⁻¹¹ One particle is to be designated as the reference particle, the dynamics of which is specified by phase space coordinates $[\mathbf{r}_{\text{ref}}(s), \mathbf{p}_{\text{ref}}(s)]$, where the independent variable s is chosen to be the arc length along its trajectory. Particle optical coordinates $Z(s) = [Z_1(s), \dots, Z_n(s)]$, where n is the dimensionality of phase space, describe variations in the other beam particles' phase space coordinates relative to those of the reference particle. It follows that $Z(s)$ is always the null vector for the reference particle. Along with many other matrix-oriented codes, COSY Infinity uses particle optical coordinates $(x, a, y, b, l, \delta_K)$ which are specified as deviations from reference particle phase space variables in the following manner: x and y are coordinates along an orthonormal frame moving with a reference particle. a and b are components of the momentum along the x and y directions, respectively, normalized by the reference particle momentum. l is a distance proportional to the difference in time of flight from the reference particle times the reference particle velocity, and δ_K is the fractional deviation in kinetic energy K from the reference particle, i.e., $\delta_K = (K - K_0)/K_0$. The evolution of the particle optical coordinates is described by a set of ordinary differential equations:

$$\frac{d}{ds} Z = f(Z, p, s),$$

where p is a set of parameters describing the system. Under mild restrictions on f , this equation has a unique solution which defines the transfer map M , describing the evolution of the coordinates Z from position s_0 to s .¹ In most cases M is only weakly nonlinear and can be represented in terms of its Taylor expansion:

$$Z_i(s) = M_{ij}^1 Z_j(s_0) + M_{ijk}^2 Z_j(s_0) Z_k(s_0) + \dots,$$

where the superscript on M_{ij}, \dots denotes the order of the expansion and repeated indices are summed. Once the transfer map is computed for a system of optical elements, the final beam coordinates can be obtained from the initial through simple polynomial evaluation.

Previous versions of COSY Infinity can evaluate arbitrary order maps only for ion-optical elements that produce no net change in particle energies. Maps of electrostatic elements such as quadrupoles and Einzel lenses were evaluated by permitting the energies to change *locally* within the elements, but it was implicit that there was no net change in the coordinate δ_K , which was taken to be a constant of the motion in the system maps. This restriction is eliminated in the present version so that beam energy changes by dc and rf electric fields are permitted. In terms of the normalized momentum

$$\frac{\mathbf{p}}{p_0} = \left(a, b, \frac{p_s}{p_0} \right),$$

using the Lorentz force law with arclength as the independent variable, we arrive at an explicit form for the dependence of δ_K on s :

$$\delta'_K = 2K_{\text{rel}} \left[aa' + bb' + \frac{p_s}{p_0} \frac{E_z v_0 t'}{\chi_{e0}} \right], \tag{1}$$

where

$$v_0 t' = \frac{\gamma}{\gamma_0} \frac{p_0}{p_s} \frac{m}{m_0},$$

and K_{rel} is a relativistic correction factor given by

$$K_{\text{rel}} = \frac{p_0 c}{2K_0} \frac{1}{\sqrt{a^2 + b^2 + (p_z/p_0)^2 + (mc/p_0)^2}}. \tag{2}$$

Equations (1) and (2) have been simplified to the case of a straight reference particle trajectory and negligible magnetic field, as is typical for the class of relatively low frequency rf and electrostatic elements we consider in the following sections. In these expressions \mathbf{p} is particle momentum, E_z is the electric field, m is the rest mass, K_0 is the reference particle kinetic energy, and the local electric rigidity of the reference particle is given by

$$\chi_{e0} = \frac{p_0 v_0}{ze},$$

where v_0 is the magnitude of the reference particle velocity and ze is the charge. The subscript zero refers to the reference particle.

Although for electrostatic accelerating elements the local value of the kinetic energy can be determined from the potential V directly as

$$K(x, y, s) = K_0 - zeV(x, y, s), \tag{3}$$

this formula is not valid for systems with time-varying electric fields. We note that in these systems it is necessary to instead determine the kinetic energy by integrating through the local electric fields.

III. MODEL FOR FIELDS OF RF AND ELECTROSTATIC STRUCTURES

A. Fields and potentials

To evaluate the elements of high-order maps for cylindrically symmetric electrostatic elements, COSY requires an analytic expression for the electrostatic potential on the axis of the element. This electrostatic potential is Taylor expanded using DA methods to obtain the off-axis terms to arbitrary order. The on- and off-axis electric field components are determined through the derivatives of the on-axis potential using DA. It is also possible to start from an expression for the electric field on axis, and use DA to Taylor expand it and obtain off-axis terms. Details of such a field expansion are provided in Appendix A, and the implementation of such expansions in DA is further discussed in Appendix B. Inaccuracies in the functional form for the field or potential on-axis can lead to unphysical terms in the Taylor expansion due to the high-order derivatives required. The approach described in Sec. III A is robust against this problem and is well suited to generating accurate high-order maps.

After determining the electrostatic field expansions, we consider simple harmonic time dependence of the form

$$\mathbf{E}(x, y, s, t) = \mathbf{E}(x, y, s) \cos(\omega t + \phi), \quad (4)$$

where induced magnetic fields from Maxwell's equation

$$\nabla \times \mathbf{B} = \frac{1}{c^2} \frac{\partial \mathbf{E}}{\partial t} \quad (5)$$

are neglected in the examples that follow. These fields are negligible for frequencies in the hundreds of megahertz and gap lengths on the order of centimeters, as is typical for heavy-ion linear accelerators. (The magnetic fields can produce significant steering effects in some types of accelerating cavities that do not have cylindrical symmetry. See Ref. 12, for example. However, these perturbations are not present in cylindrically symmetric cavities.)

B. Accurate cavities and electrostatic lenses

In the past it has been common to use an approximate analytical fit to the numerical expression for the potential on axis of an Einzel lens.¹¹ However, this expression is not appropriate for higher order maps since small errors in this approximation are greatly amplified in the Taylor expansion involving its derivatives. To reduce the resulting errors in off-axis fields, the map-optics code can take as input an analytic expression for an axial potential due to rings of charge at the surfaces of the cylindrical electrodes located off-axis. The charge densities on the rings are determined through a Poisson solver by using the equivalent potential boundary condition. The fields of a typical element are represented quite well by subdividing the electrodes into 100 or more charge rings. The resulting axial potential is robust against small errors in these determined charge densities, and consequently a more exact expression for the axial potential is obtained. Thus the growth of error with increased differentiation is greatly reduced. To facilitate the use of this method in COSY, a Poisson solver based on the method of moments

has been incorporated. Given a particular cavity geometry, the resulting potential on axis can be determined all within the modified program.

The Poisson solver relies on the routine "CYLEST" written previously by one of us (K.W.S.). Given a set of cylindrically symmetric electrodes taken as equipotentials, the solver determines the charge densities on the surfaces of these electrodes. The electrodes are approximated by a sequence of ring segments (r_i, z_i, δ_i) where δ_i is the width of the i th segment. The electrostatic potential ϕ is given by

$$\phi(\mathbf{r}) = \frac{1}{4\pi\epsilon_0} \sum_i \int \frac{\sigma_i}{|\mathbf{r} - \mathbf{r}'|} dA'_i, \quad (6)$$

where the sum is performed over each ring segment with charge density σ_i and area dA_i . Given ϕ on the boundary, Eq. (6) is an integral equation in the unknown σ . Employing cylindrical coordinates (r, θ) , we can write

$$\phi(\mathbf{r}) = \frac{1}{4\pi\epsilon_0} \sum_i Q_i \frac{1}{2\pi} \times \int_0^{2\pi} \frac{d\theta}{[r^2 + r_i^2 - 2rr_i \cos \theta + (z - z_i)^2]^{1/2}}, \quad (7)$$

where the charge on the i th segment is $Q_i = 2\pi r_i \delta_i \sigma_i$. Making a change of variables, we find

$$\phi(\mathbf{r}) = \frac{Q_i}{\pi(B_i + C_i)^{1/2}} \int_0^\pi \frac{d\psi}{1 - (2C_i/B_i + C_i) \cos \psi^2} \quad (8)$$

with $B_i = r^2 + r_i^2 + (z - z_i)^2$ and $C_i = 2rr_i$ and $\psi = \theta/2$. The integral is simply twice the complete elliptic integral of the first kind $K(\kappa)$ with $\kappa = (2C_i/B_i + C_i)^{1/2}$.¹³ By evaluating the potential $\phi(\mathbf{r})$ on the surface of the j th electrode at $\mathbf{r} = (r_j, z_j)$ we can write the above equation as a matrix:

$$\phi_j = \frac{1}{4\pi\epsilon_0} \sum_i P_{ij} Q_i. \quad (9)$$

Care must be taken for the diagonal term $i=j$, which is handled by splitting the ring into two regions: The first contains the contribution

$$\phi_{ii}^{(1)} = \frac{1}{4\pi\epsilon_0} Q_i \int_{\delta_i/2r_i}^{2\pi - (\delta_i)/2r_i} \frac{d\theta}{(2r_i^2 - 2r_i^2 \cos \theta)^{1/2}} \quad (10)$$

and the second contribution is evaluated by replacing the remaining unintegrated square by a circle of equivalent charge, so

$$\phi_{ii}^{(2)} = \frac{1}{4\pi\epsilon_0} \int_0^{\delta_i/\sqrt{\pi}} \frac{2\pi r dr}{r} \sigma_i. \quad (11)$$

The sum results in the diagonal component of P :

$$P_{ii} = \left[\sqrt{\pi} + \ln \left(\frac{16\pi r_i^2}{A_i} \right) \right] / (\pi r_i). \quad (12)$$

The matrix P can be inverted to obtain the resulting charge on each ring:

$$Q_i = 4\pi\epsilon_0 \sum_j P_{ij}^{-1} \phi_j. \quad (13)$$

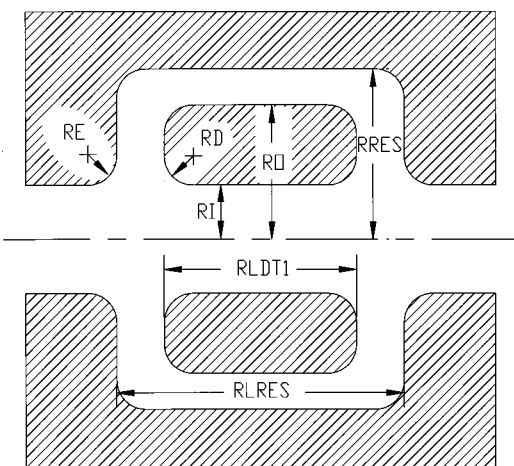


FIG. 1. Accurate two-gap cavity geometrical parameters for user input.

A typical two-gap cylindrical lens or cavity is illustrated in Fig. 1 and later utilized for beam-optics calculations. Realistic dimensions including electrode corner radii can be specified as indicated. Reference 14 contains a complete listing of this procedure. Other types of cylindrically symmetric cavities such as one-gap, three-gap, or four-gap structures have also been included by extending the Poisson solver to such parametrizations. For brevity, these will not be further elaborated in this article.

IV. BEAM DYNAMICS COMPARISON WITH RAY TRACING

In order to verify the changes to the map-optics formalism that permit calculation of rf structures, a comparison with ray tracing was carried out. To facilitate the comparison, a two-gap cylindrical resonator is modeled according to the nominal parameters listed in Table I. The potential on-axis is taken as the analytic expression for the superposition of hundreds of charged rings, with corresponding charge density determined by the Poisson solver. The same electrode geometry was used in the ray-tracing code SIMION 6.0,¹⁵ which solves Laplace’s equation via relaxation techniques on a grid to determine the on- and off-axis electrostatic potentials and fields. Charged particle trajectories are then numerically integrated using the local electric fields. Although the charged rings used by COSY and the geometry used in SIMION extend

TABLE I. Nominal parameters for two-gap cavity comparison with ray tracing.

Quantity	Symbol	Nominal value
Beam energy	K_0	0.33 MeV
Mass	M_0	10 amu
Charge	Z_0	+1
Velocity/c	β	0.008 419
Inner tube radius	ri	0.01 m
Outer tube radius	ro	0.02 m
Resonator radius	$rres$	0.03 m
Radii of curvature	re	0.002 m
Center tube length	$rldt1$	0.067 m
Resonator length	$rlres$	0.1 m
Peak tube voltage	n_p	0.1112 MV
Radio frequency	ν	15.114 MHz

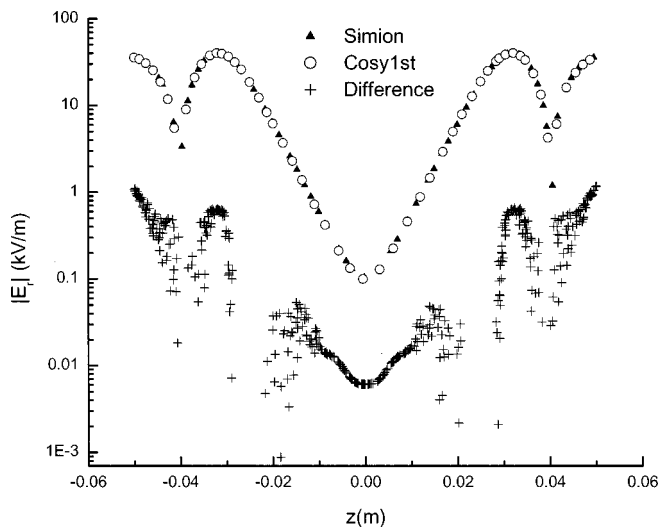


FIG. 2. Comparison of radial electric field at 1/50 radius off axis between SIMION and COSY to first order.

for one inner radius beyond the resonator wall, SIMION prescribes an equipotential boundary condition at this location in z . Thus, to avoid boundary effects, the comparison is carried out only within the resonator itself, from the start of the first gap until the end of the second gap. The axial potential and electric fields calculated by COSY and SIMION agree nearly exactly, as expected, and the transverse electric field slightly off-axis agrees very well as shown in Fig. 2. The very slight differences may be due in part to finite grid size effects, either in numerical differentiation of the potential or specification of the boundary conditions, as well as the tolerance chosen for convergence of the relaxation method, taken to be one part in 10 000. At half of the inner tube radius, the transverse electric field off axis up to fifth order is shown in Fig. 3. The peak field is nearly 20% off at first order, but the COSY result converges toward the SIMION value as the order of the expansion is increased, as expected.

After establishing agreement for the electrostatic fields inside the resonator, a comparison of the dynamics in the

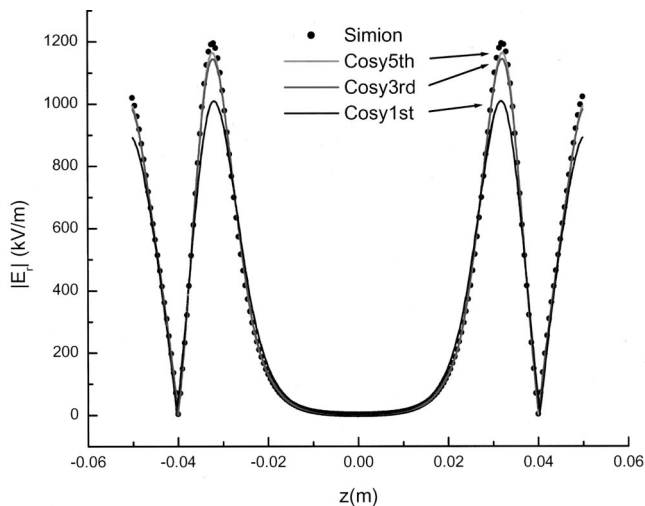


FIG. 3. Comparison of radial electric field at 1/2 radius off axis between SIMION and COSY.

TABLE II. Comparison of longitudinal and transverse perturbations for electrostatic case with initial offset less than one-tenth cavity radius.

Matrix element	COSY	SIMION	Deviation (percent)
$(x x)$	0.6907	0.6934	0.39
$(a x)$ (rad/m)	-5.316	-5.271	0.85
$(l xx)$ (m^{-1})	-12.3	-12.5	1.6

electrostatic case was performed. Again using beam parameters as in Table I, the effect of initial displacement x on final beam coordinates x , a , and l was calculated to third order in COSY and compared with SIMION. For small initial transverse perturbations, within $\approx 1/10$ radius results are shown in Table II. Agreement is better than 1% between SIMION and first-order matrix elements in COSY. The slight effect of the second-order matrix element $(l|xx)$ also agrees within 2%. The slight discrepancy may be attributed to the fact that matrix elements are obtained from SIMION through numerical differentiation of final ray coordinates, while COSY obtains them directly via DA integration of the transfer map.¹ Also, small differences in the electric fields as shown in Fig. 2 may contribute.

For larger initial displacement (half-radius), inclusion of the third-order term $(x|xxx)$ reduces the deviation in the magnification from 1.17% at first order to 0.21%. The third-order aberration term $(a|xxx)$ characterizes a change in the effective focal length of the lens. Inclusion of this term restores agreement for the exit angle of incident parallel rays at half-radius from roughly 2% to better than 1%. This is due to the increased agreement in transverse electric field at third order as shown in Fig. 3, as well as to the general improvement in geometric optics at higher order.

In order to accurately calculate optics for beams which fill half or more of the aperture, third-order terms become essential. For example, at 70% of the full aperture, the effect of the aberration term $(a|xxx)$ becomes a 5.1% correction to the exit angle, and including it restores agreement with ray tracing to within 1%. The fifth-order correction $(a|xxxxx)$ at this large initial displacement also becomes sizable at 0.61%. The matrix elements for these aberrations and their contributions relative to the first-order term are listed in Table III.

Given this agreement for the electrostatic case, a comparison of dynamics was done for the full time-varying case. This example is typical of a two-gap, low-beta superconducting resonator. Chosen for comparison were the reference particle energy gain versus cavity phase, and the dependence of the bunch length coordinate l on initial energy offset δ_K . As Fig. 4 indicates, results are in good agreement for both quantities.

V. APPLICATIONS

A. Accurate electrostatic lenses and accelerating gaps in map optics

The need for accurate calculation of electrostatic lenses has been long since recognized,¹⁶⁻¹⁸ and there is a rich history of low-order treatment of them.^{11,19-22} The conventional calculation of formulas for higher order aberrations is exceedingly difficult and thus has not been developed.¹⁹ For

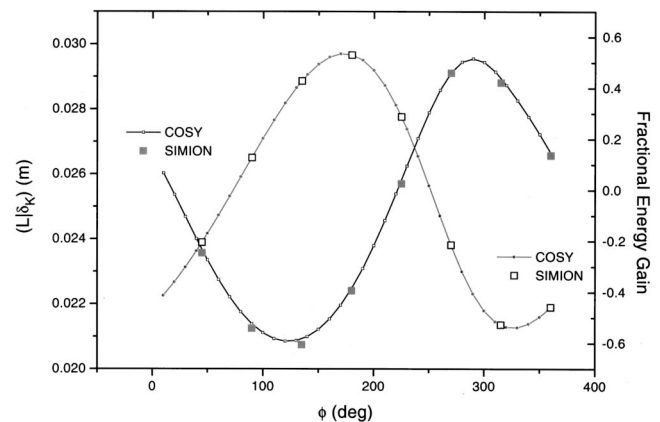
TABLE III. Contributions of angular aberrations at 70% aperture relative to first order.

Matrix element	Value	Contribution at 0.70 aperture
$(a x)$ (rad/m)	-5.316	1.000
$(a x^3)$ (rad/m ³)	-5.533E3	0.051
$(a x^5)$ (rad/m ⁵)	-1.328E7	0.006

example, first-order matrix-optics has been provided for single gap lenses under asymptotic approximations, but due to the lack of accurate estimates of nonlinear aberrations and a restricted class of geometries, these results are of limited applicability. More accurate calculations of geometric aberrations in electrostatic lenses using a charged-ring approach similar to the one we employ have been previously performed for certain geometries.^{17,18} Despite this, electrostatic lenses have formerly been implemented in *matrix* codes only as rough approximations, and again only to low order and for specialized geometries. Our formulation permits for the first time the implementation of accurate electrostatic lenses, in particular the two-gap ‘‘Einzel’’ lens, in an arbitrary-order general-purpose map-oriented beam-optics code. The geometry of the lens can be chosen with great flexibility including parameters such as the radii of curvature, and the associated axial potential can be determined accurately as an analytic expression. This expression can be differentiated precisely using DA methods to provide accurate off-axis (lensing) fields and their associated aberrations, within the map-optics formalism. Further, one can readily fit lens geometry and voltage to obtain desired optics.

B. The Rare Isotope Accelerator Facility

Designs of several subsystems for the Rare Isotope Accelerator Facility (RIA)²³ are currently underway at Argonne. Two ion-optical systems for RIA are being designed using the new higher order elements made possible by the present work. One of these is a large-acceptance, high-resolution isobar separator that includes an imaging and decelerating electrostatic section to permit energy-spread compensation.²⁴ To achieve the desired mass resolving power of 20 000 this system must be calculated to fifth order. The second of these

FIG. 4. Comparison of fractional energy gain and matrix element $(l|\delta_K)$ between SIMION and COSY.

systems is the beam transport between driver linac sections following stripping of heavy ions to higher charge states. This section must be achromatic and isochronous (equal path lengths for all charge states), as well as, provide the rf rebunching for matching into the down stream linac section.²⁵ Fitting the six-dimensional beam ellipses for all these constraints is enabled by the newly implemented higher order map elements for superconducting rf cavities.

C. Optimizing rf structures and lattices

As an alternative to ray tracing through a large amount of phase space by trial and error, the fitting algorithms of COSY can be implemented to obtain desired bunching or energy gain conditions in order to optimize a lattice of resonators. As a simple example of how the code can be utilized, we consider the optimization of a system consisting of three magnetic solenoids separated by independently phased rf cavities. Table I describes the initial beam used for the test case. The solenoids can be calculated using an existing algorithm provided in the code. A beam passing through a rf cavity experiencing acceleration and longitudinal bunching can in general simultaneously experience a transverse defocusing. By placing magnetic solenoids and rf cavities in a lattice structure, additional transverse focusing can be achieved to counteract this effect. Using COSY, it is possible to fit the magnetic field strength in each solenoid independently in order to minimize the transverse beam envelope in the center of the rf cavity that follows it.

The transfer map for the first solenoid is computed to first order, and the magnetic field strength is fit to the value providing a first-order image at the center position where the following resonator will be placed. The map can then be computed to second or higher order in a single iteration.

As an alternative method, a distribution of randomly selected rays from a given initial beam emittance profile can be calculated to second or higher order as it travels through the solenoid, and iterations can be performed in order to minimize the transverse beam envelope as a function of magnetic field. This method is slightly more time consuming as it involves performing iterations each involving the determination of higher order transfer maps. For cases tested previously,²⁶ both methods have produced comparable optimal magnetic field strengths.

Once the optimized transfer map for the first solenoid is calculated, it can be stored and reapplied to the initial beam vector in order to fit the composition transfer map for the following resonator and the solenoid without having to recalculate the transfer map for the solenoid during each iteration. The phase corresponding to maximal energy gain was determined and this phase was then offset by a nominal amount to provide bunching. The resonator map was subsequently calculated to second order. This composed map was then stored and used in a fitting loop to optimize the map of the composition of the first solenoid, the resonator, and the second solenoid, without having to recompute the map for the first two. This procedure was carried forth in similar fashion for the second resonator and the third solenoid and the times involved were comparable. Since the fitting for the magnetic

solenoids can be done at first or second order and the fitting for the rf cavities can be done to first order, the time scale involved is fairly reasonable. These lower order solutions can be fine-tuned to third and higher order if desired.

VI. DISCUSSION

We have developed a formulation of an arbitrary-order map-oriented beam optics code which implements a class of rf and electrostatic structures intended for particle acceleration, bunching, and focusing. The implementation of rf structures in a map-optics formalism provides advantages for repeated occurrence of particle optical elements and for fitting on system parameters. Inclusion of higher order maps allows straight-forward optimization with respect to nonlinearities. Field models for high accuracy evaluation of the Taylor maps of cylindrically symmetric electrostatic lenses (zero rf frequency) and time-varying cavities have been provided. The map formulation was compared with ray-tracing calculations to illustrate the importance of higher order terms. Examples of ion-optical systems currently under design using the elements enabled by the present work were given.

ACKNOWLEDGMENTS

The authors thank Weshi Wan for helpful remarks. This work is supported by the U.S. DOE under Contract Nos. W-31-109-ENG-38 and DE-FG02-95ER40931.

APPENDIX A: FIELD EXPANSIONS

We adopt cylindrical coordinates (r, ϕ, z) and begin with an expression for the axial electric field $a_0(z)$. In charge free regions, we have

$$\frac{1}{r} \frac{\partial}{\partial r} (rE_r) + \frac{\partial E_z}{\partial z} = 0, \quad (\text{A1})$$

$$\frac{\partial E_r}{\partial z} - \frac{\partial E_z}{\partial r} = 0. \quad (\text{A2})$$

Assuming a solution of the form

$$E_z = \sum_n a_{2n} r^{2n}, \quad (\text{A3})$$

$$E_r = \sum_n b_{2n} r^{2n+1} \quad (\text{A4})$$

leads to a recurrence relation

$$a_{2n+2} = \frac{-1}{(2n+2)^2} a_{2n}''', \quad (\text{A5})$$

$$b_{2n} = \frac{-1}{(2n+2)} a_{2n}'', \quad (\text{A6})$$

where a and b are functions of z only and primes denote differentiation with respect to z . As we expect by symmetry, the axial component of the electric field depends only on even powers of r and the radial component depends only on odd powers of r . This expansion method can also be applied beginning with a potential V on axis, since

$$a_0(z) = -V'. \quad (\text{A7})$$

APPENDIX B: IMPLEMENTATION IN DA

In this Appendix, we discuss the implementation of field expansions such as those described in Appendix A within the DA formalism. These field expansions and recursion relations can be explicitly executed to determine the off-axis fields. However, for practical arbitrary order calculations using DA as in current map codes, the treatment of the actual solution of the ODE for the potentials and fields is reformulated to avoid the need for coding of high-order derivatives of a_{2n} with respect to s and the need to execute the recursion relations explicitly. Thus the method has the advantage that it works to any order outright.

Even though Appendix A describes an expansion in two-dimensional geometry, as is adequate for the cylindrically symmetric elements we consider, the DA method is applicable for general 3D motion with or without midplane symmetry as long as the fields are known. In the general setting of the Laplacian Δ^C in 3D curvilinear coordinates (x, y, s) (see Ref. 2) we have

$$\Delta^C f = \frac{1}{\alpha} \left(\frac{\partial}{\partial s} + \tau_1 y \frac{\partial}{\partial x} - \tau_1 x \frac{\partial}{\partial y} \right) \left[\frac{1}{\alpha} \left(\frac{\partial f}{\partial s} + \tau_1 y \frac{\partial f}{\partial x} - \tau_1 x \frac{\partial f}{\partial y} \right) \right] + \frac{1}{\alpha} \frac{\partial}{\partial x} \left(\alpha \frac{\partial f}{\partial x} \right) + \frac{1}{\alpha} \frac{\partial}{\partial y} \left(\alpha \frac{\partial f}{\partial y} \right),$$

where τ_1 is the rate of rotation around \mathbf{e}_s , τ_2 and τ_3 are the curvatures in $\mathbf{e}_y - \mathbf{e}_s$ and $\mathbf{e}_x - \mathbf{e}_s$ planes, respectively, and $\alpha = 1 - \tau_3 x + \tau_2 y$. Performing some partial integrations, the expression can be rewritten as a fixed point problem

$$f = f_{y=0} + \partial_y^{-1} \left[\frac{1}{\alpha} \left(\alpha \frac{\partial f}{\partial y} \right) \right]_{y=0} - \partial_y^{-1} \left[\frac{1}{\alpha} \partial_y^{-1} \left\{ \frac{\partial}{\partial x} \left(\alpha \frac{\partial f}{\partial x} \right) \right\} \right] - \partial_y^{-1} \left[\frac{1}{\alpha} \partial_y^{-1} \left\{ \left(\frac{\partial}{\partial s} + \tau_1 y \frac{\partial}{\partial x} - \tau_1 x \frac{\partial}{\partial y} \right) \left\{ \frac{1}{\alpha} \left(\frac{\partial f}{\partial s} + \tau_1 y \frac{\partial f}{\partial x} - \tau_1 x \frac{\partial f}{\partial y} \right) \right\} \right\} \right].$$

This representation of Laplace's equation has the following important property. If f as well as its first partial $\partial_y f$ are known to order n in x and s , and furthermore f is known to order $\nu < n$ in y , then applying the right-hand side of the fixed point equation to f yields the dependence on y to order $\nu + 1$. This is due to the fact that the right-hand side contains two integrations with respect to y , both of which raise the order ν to which f is known in y , but only one differentiation

with respect to y . The also occurring differentiations with respect to x and s have no influence on ν and are possible because we assume to know f to order n in x and s . So in practical DA computations, one begins with a DA vector that contains only the midplane derivatives of the potentials, which can be obtained by evaluating the respective formulas in Sec. III with DA. Then, iterating the expression thus automatically fills up the order to which the dependence is known in the y direction in an order-by-order manner.

- ¹M. Berz, *Modern Map Methods in Particle Beam Physics* (Academic, San Diego, 1999).
- ²K. Makino and M. Berz, *Int. J. Appl. Math.* **3,4**, 421 (2000); M. Berz and K. Makino, *ibid.* **3,4**, 401 (2000); K. Makino, Ph.D. thesis, Michigan State University East Lansing, MI, 1998.
- ³K. L. Brown, R. Belbeoch, and P. Bounin, *Rev. Sci. Instrum.* **35**, 481 (1964).
- ⁴K. L. Brown, The Ion Optical Program TRANSPORT, SLAC Tech.-Pub. 91, 1979.
- ⁵T. Matsuo and H. Matsuda, *Mass Spectrosc. (Tokyo)* **24**, 19 (1976).
- ⁶H. Wollnik, *Optics of Charged Particles* (Academic, Orlando, FL, 1987).
- ⁷D. C. Carey, *The Optics of Charged Particle Beams* (Harwood Academic, New York, 1987, 1992).
- ⁸A. J. Dragt and J. M. Finn, *J. Math. Phys.* **17**, 2215 (1976).
- ⁹A. J. Dragt, *AIP Conf. Proc.* **87**, 147 (1982).
- ¹⁰A. J. Dragt, L. M. Healy, F. Neri, and R. Ryne, *IEEE Trans. Nucl. Sci.* **NS-3,5**, 2311 (1985).
- ¹¹X. Jiye, *Aberration Theory in Electron and Ion Optics* (Academic, New York, 1986).
- ¹²P. N. Ostroumov and K. W. Shepard, *Phys. Rev. ST Accel. Beams* **4**, 110101 (2001).
- ¹³M. Abramowitz and I. A. Stegun, *Handbook of Mathematical Functions* (Dover, New York, 1965, 1972), originally published by National Bureau of Standards in 1964.
- ¹⁴COSY Infinity Web Page and Manual. <http://bt.nsl.msui.edu/cosy>
- ¹⁵SIMION 6.0, SIMION 7.0, Ion Source Software, P.O. Box 2726, Idaho Falls, ID 83403, <http://www.srv.net/~klack/simion.html>
- ¹⁶J. D. Larson, *Nucl. Instrum. Methods* **189**, 71 (1981).
- ¹⁷G. Martinez *et al.*, *Nucl. Instrum. Methods Phys. Res. A* **363**, 198–204 (1995).
- ¹⁸D. DiChio *et al.*, *Rev. Sci. Instrum.* **45**, 566 (1974).
- ¹⁹P. W. Hawkes and E. Kasper, *Principles of Electron Optics*, 1–2 (Academic, London, 1989).
- ²⁰M. Szilagy, *Electron and Ion Optics* (Plenum, New York, 1988).
- ²¹*Lie Methods in Optics*, edited by K. B. Wolf (Springer, Heidelberg, 1989).
- ²²M. Born and E. Wolf, *Principles of Optics*, 6th ed. (Pergamon, Oxford, 1980).
- ²³G. Savard, Proceedings of the 2001 IEEE Particle Accelerator Conference, Chicago, 2001.
- ²⁴M. Portillo, J. A. Nolen, and T. A. Barlow, Proceedings of the 2001 IEEE Particle Accelerator Conference, Chicago, 2001, p. 2876.
- ²⁵M. Portillo, V. N. Aseev, J. A. Nolen, and P. N. Ostroumov, Proceedings of the 2001 IEEE Particle Accelerator Conference, Chicago, 2001, p. 2873.
- ²⁶A. Geraci *et al.*, University of Chicago Senior thesis, 1998 (unpublished).